

Modeling the Preferred Shapes of Polyamine Transporter Ligands and Dihydromotuporamine-C Mimics: Shovel versus Hoe

Fred Breitbeil III,[†] Navneet Kaur,[‡] Jean-Guy Delcros,[‡] Bénédicte Martin,[‡] Khalil A. Abboud,[§] and Otto Phanstiel IV*[‡]

Groupe Cycle Cellulaire, CNRS UMR 6061, IFR 97, Facult de Medecine, Universit Rennes 1, 2 Av. du Pr Leon Bernard, CS 34317, F-35043 Rennes Cedex, France, Department of Chemistry, University of Florida, Gainesville, Florida 32611, and Department of Chemistry, University of Central Florida, P.O. Box 162366, Orlando, Florida 32816-2366

Received August 16, 2005

Preferred conformers generated from motuporamine and anthracene–polyamine derivatives provided insight into the shapes associated with polyamine transporter (PAT) recognition and potentially dihydromotuporamine C (**4a**) bioactivity. Molecular modeling revealed that *N*¹-(anthracen-9-ylmethyl)-3,3-triamine (**6a**), *N*¹-(anthracen-9-ylmethyl)-4,4-triamine (**6b**), *N*¹-(anthracen-9-ylmethyl)-*N*¹-ethyl-3,3-triamine (**7a**), *N*¹-(anthracen-9-ylmethyl)-*N*¹-ethyl-4,4-triamine (**7b**), and **4a** all preferred a hoe motif. This hoe shape was defined by the all-anti polyamine shaft extending above the relatively flat, appended ring system. The hoe geometry was also inferred by the ¹H NMR spectrum of the free amine of **7a** (CDCl₃), which showed a strong shielding effect of the anthracene ring on the chemical shifts associated with the appended polyamine chain. This shielding effect was found to be independent over a broad concentration range of **7a**, which also supported an intramolecular phenomenon. The degree of substitution at the *N*¹-position seems to be an important determinant of both the molecular shape preferences and biological activity of anthracenylmethyl–polyamine conjugates.

Introduction

The shape of a molecule plays an important role in its biological function. Shape mimicry is, therefore, a key feature of drug design. Natural product drug candidates are often cocrystallized with their putative biological target in order to understand the intermolecular contacts involved between the substrate and the biotarget. In the absence of said crystals, one can use molecular modeling to identify the “preferred” conformers of drug candidates and infer that these same shapes may be involved in their biological function. Subsequent synthesis of the structurally related, shape mimic allows one to test whether the “preferred” shape invokes a similar biological response.

In this report, the motuporamines¹ were investigated by molecular modeling in hopes of identifying a molecular shape associated with their unique anticancer and anti-invasion properties.² The motuporamines are natural polyamines isolated from *Xestospongia exigua*, a sea sponge collected from the outer reef of Motupore Island, Papua New Guinea.¹ The native motuporamines **1–3** each contain a large hydrophobic heterocycle appended to a polyamine motif (Figure 1). Indeed, dihydromotuporamine C (**4a**), which contains a 15-membered macrocycle attached to a 3,3-triamine motif, has demonstrated high cytotoxicity against MDA-231 breast carcinoma cells and good anti-invasive properties with tumor cells.² In addition, a simple carbazole derivative **5** was shown to have good anti-invasive properties by Andersen et al.^{2a}

Prior work in our laboratories and others have revealed the structural requirements associated with the delivery of polyamine conjugates via the polyamine transporter (PAT) in L1210 and CHO cells.^{3–12} In short, the methylene spacer units (Figure 1, **6**: *x*, *y*, and *z*), the size of the *N*¹-substituent, and the degree of

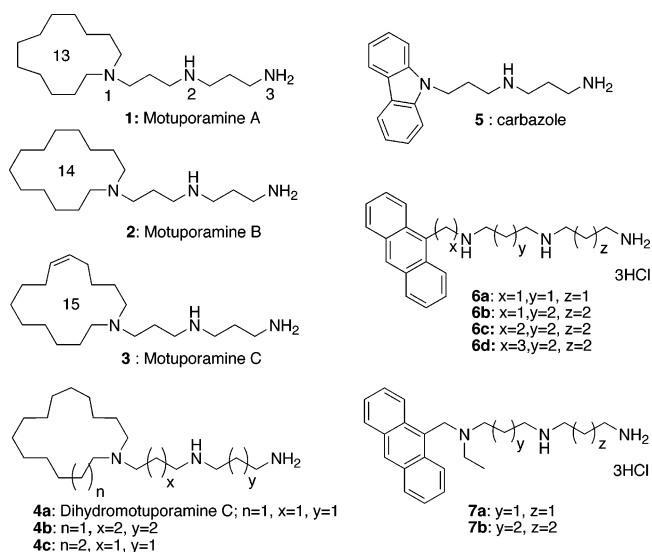


Figure 1. Structures of Motuporamines A–C (**1–3**) and polyamine derivatives **4–7**.

*N*¹-substitution all influence PAT-mediated delivery.^{3,5,7,8} Moreover, a recent report from our laboratories revealed that the dihydromotuporamine C adducts (**4a** and **4b**) and *N*¹-ethyl-*N*¹-anthracenylmethyl-homospermidine **7b** do not use the polyamine transporter (PAT) for cellular entry.³

At first glance, these two issues (PAT selectivity and motuporamine mimicry) do not seem related. However, we have discovered that they are intimately related. For example, *N*¹-ethylation of **6b** (a highly selective PAT ligand) creates **7b**, which is not PAT selective.³ In addition, *N*¹-ethylation of **6a** creates **7a**, which has similar shape and initial biological activity as dihydromotuporamine C (**4a**). In this manner *N*¹-ethylation was shown to be responsible for both loss of PAT selectivity and induction of **4a** mimicry.

Having shown that tertiary amine centers at the *N*¹-position were not preferred by the PAT,³ we initiated a molecular

* Corresponding author. Phone: (407) 823-5410. Fax: (407) 823-2252. E-mail: ophansti@mail.ucf.edu.

[†] University of Central Florida.

[‡] University of Florida.

[§] University of Rennes 1.

modeling study to better understand the shape preferences of the motuporamines (**1–4**), their mimic **5**, and potential new mimics **7**. Indeed, it was not unreasonable to assume that an alternative architecture like **7** could elicit the same response as **4a**, because carbazole **5** had already been shown to have properties similar to those of **4a**.^{2a}

Our goal was to further refine our earlier PAT-selectivity model⁸ by identifying the preferred conformers of both PAT-selective systems (like **6**) and PAT-nonselective systems (like **4** and **7**). Since **4a** was not amenable to NMR investigation,^{2a} we hoped to use the related mimics **7** to understand the potential shape preferences of **4**. This seemed reasonable as neither **4a,b** nor **7b** were PAT-selective and the respective homospermidine derivatives (**4b** and **7b**) had similar cytotoxicity profiles in L1210 cells.³

Indeed, distinctive conformational preferences and molecular shapes (i.e., hoe and shovel motifs) were observed for these systems (**1–7**). The calculated molecular shapes also correlated well with previous PAT selectivity and the cytotoxicity results.^{3,8} In prior studies, the norspermidine derivative **4a** was found to be more cytotoxic than the homospermidine derivative **4b**.³ Therefore, it seemed reasonable to assume that a related norspermidine analogue **7a** would be more cytotoxic than **7b**. As a result, **7a** became an important synthetic target and provided a new shape mimic of **4a** to evaluate by ¹H NMR studies.

In terms of mimic design, the motuporamines are problematic and typically give broad ¹H NMR spectra, which hinder investigation of their solution-phase conformational preferences and determination of their bioactive shape.^{2a} In an earlier report Andersen concluded that **4a** “exists as a mixture of interconverting conformations in solution at room temperature”.²

Therefore, acquiring new shape mimics of **4a** was important for several reasons. First, we hoped to improve upon the cytotoxicity and anti-invasive properties of **4a** and **5**^{2a} using readily accessible derivatives such as **7a**. Second, a determination of the preferred shapes of PAT selective and PAT nonselective ligands (**6b** and **7b**, respectively) would help to further refine our earlier PAT model.⁸ Third, the new mimics **7** were more amenable to inspection by ¹H NMR because the “conformationally mobile” macrocycle in **4a** was now “sequestered” as an anthracene ring in **7a**.

Indeed, preliminary modeling studies suggested that a tertiary amine center at the N¹-position preferred to direct the attached polyamine chain (in **4a,b** and **7**) over its respective macrocycle.

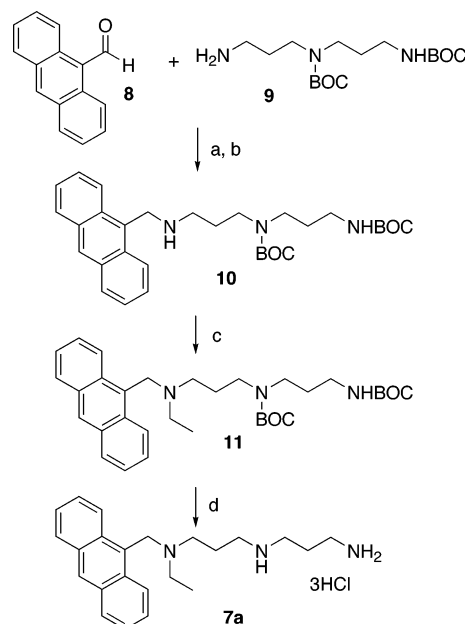
Since similar geometries were predicted for both **4a** and **7a**, we envisioned using the anthracene ring system as a “reporting-surrogate” macrocycle in the ¹H NMR studies. Due to the inherent shielding effects associated with the anthracene π -system, the chemical shifts of the polyamine methylene chain are significantly upfield, when the chain is oriented over the anthracene ring.¹³ Comparison of the chemical shifts observed with **6a,b** and **7a,b** provided support for their computationally modeled shape preferences. In summary, ¹H NMR studies (in CDCl₃) of **6**, **7**, and other related model systems confirmed these preferred orientations by monitoring the influence of the anthracene “shielding cone” on the appended polyamine chain.

To accomplish these insights, we initiated the synthesis of **7a**, molecular modeling of these systems, and ¹H NMR studies of several anthracene–polyamine conjugates.

Results and Discussion

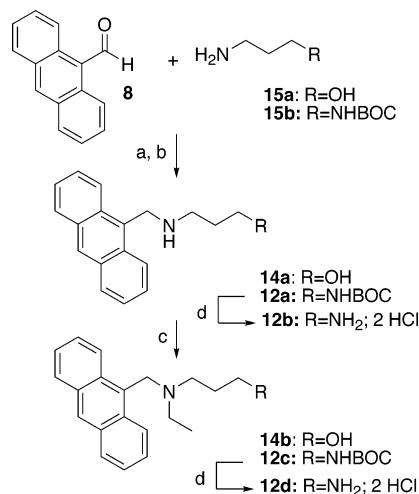
Synthesis. The new conjugate **7a** was synthesized in order to test for dihydromotuporamine C mimicry. In addition, **7a**

Scheme 1^a



^a Reagents: (a) 25% MeOH/CH₂Cl₂; (b) 50% MeOH/CH₂Cl₂, NaBH₄; (c) K₂CO₃, CH₃CN, C₂H₅Br; (d) 4 N HCl/EtOH.

Scheme 2^a



^a Reagents: (a) 25% MeOH/CH₂Cl₂; (b) 50% MeOH/CH₂Cl₂, NaBH₄; (c) K₂CO₃, CH₃CN, C₂H₅Br; (d) 4 N HCl/EtOH.

and other amino alcohol derivatives allowed for later ¹H NMR spectral comparisons. As shown in Scheme 1, our approach allowed for the rapid construction of **7a** using established methods in good yield.³

Compound **7a** was synthesized from the commercially available aldehyde **8**. The di-Boc-protected amine **9** (Boc = *tert*-butyloxycarbonyl) was synthesized using methods described in earlier reports.^{14a,c} As shown in Scheme 1, reductive amination¹⁴ of aldehyde **8** with amine **9** gave di-Boc-protected **10** (75%), which in turn was alkylated with EtBr to give the *N*-ethyl derivative **11** (80%). Treatment with 4 N HCl provided compound **7a** (90%).

As shown in Scheme 2, the synthesis of **12a–d** began with the coupling of aldehyde **8** and mono-Boc protected, 1,3-propanediamine (**15b**) to give **12a** (75%). A portion of **12a** was then treated with 4 N HCl to give **12b** as its HCl salt (90%). Another portion of **12a** was alkylated with EtBr to give the *N*-ethyl derivative **12c** (80%) and subsequently deprotected with 4 N HCl to give **12d** (90%).

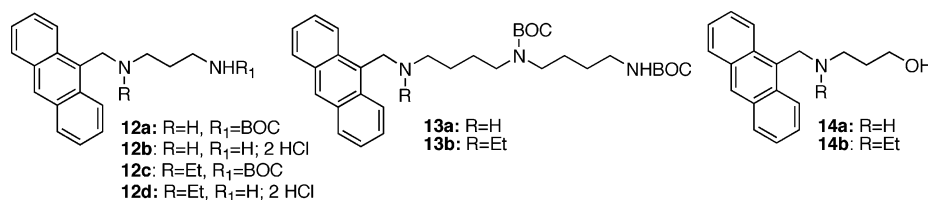


Figure 2. ^1H NMR models **12**–**14**.

Table 1. Biological Evaluation of Polyamine Derivatives in L1210, CHO, and CHO-MG Cells

compd (tether)	L1210		ref ^a	IC ₅₀ (M)		IC ₅₀ ratio ^b
	IC ₅₀ (M)	K _i value (M)		CHO-MG	CHO	
4a : dihydroMotu (3,3) ^c	3.0 ± 0.5	9.9 ± 0.5	3	10.0 ± 2.6	10.5 ± 1.6	1
4b : dihydroMotu (4,4)	18.5 ± 2.9	6.2 ± 0.5	3	28.2 ± 5.6	30.0 ± 4.1	1
6a : Ant-CH ₂ (3,3) ^d	1.8 ± 0.4	33.4 ± 2.6	5	3.4 ± 0.5	1.9 ± 0.4	1.8
6b : Ant-CH ₂ (4,4)	0.30 ± 0.04	1.8 ± 0.1	5	66.7 ± 4.1	0.45 ± 0.10	148
6c : Ant-CH ₂ CH ₂ (4,4)	3.5 ± 0.7	1.6 ± 0.1	8	33.5 ± 7.1	9.8 ± 1.1	3.4
6d : Ant-CH ₂ CH ₂ CH ₂ (4, 4)	76.3 ± 4.8	1.1 ± 0.1	8	130.8 ± 5.5	130.1 ± 7.1	1
7a : N ¹ -ethyl-N ¹ -Ant-CH ₂ (3,3)	2.2 ± 0.1	23.5 ± 0.9		4.0 ± 0.3	5.3 ± 0.4	0.8
7b : N ¹ -ethyl-N ¹ -Ant-CH ₂ (4,4)	22.2 ± 1.2	24.4 ± 1.5	3	21.9 ± 0.9	22.2 ± 0.7	1

^a Denotes the reference number in which the data was originally reported. A blank in the ref column denotes new data. Cells were incubated for 48 h with the respective conjugate; see Experimental Section. ^b The IC₅₀ ratio denotes the (CHO-MG/CHO) IC₅₀ ratio, a measure of PAT selectivity. ^c dihydroMotu = dihydromotuporamine. ^d Ant = anthracen-9-yl.

Other analogues (**13a,b**) were previously synthesized^{3,5,6} and provided excellent model compounds to further elucidate the NMR features associated with their preferred orientation. In addition, the amino alcohols **14a** and **14b** were synthesized to clearly illustrate the upfield shift associated with the anthracene shielding cone (see Supporting Information). As shown in Scheme 2, amino alcohol **14a** was synthesized by reductive amination of **8** using **15a** in 75% yield. The *N*-ethyl derivative **14b** was synthesized by *N*-alkylation of **14a** with EtI in acetonitrile (80% yield). These compounds are listed in Figure 2.

Bioevaluation. As shown in Table 1, excellent biological mimicry (e.g., L1210 cytotoxicity) of the dihydromotuporamines **4a** and **4b** were obtained with mimics **7a** and **7b**, respectively.

Chinese hamster ovary (CHO) cells were chosen along with a mutant cell line (CHO-MG) in order to comment on how the synthetic conjugates gain access to cells.³ The CHO-MG cell line is polyamine-transport deficient and was isolated after selection for growth resistance to methylglyoxalbis(guanyldrazone) (MGBG, CH₃C[=N–NHC(=NH)NH₂]CH[=N–NHC(=NH)NH₂]) using a single-step selection after mutagenesis with ethylmethanesulfonate.^{3,8}

For the purposes of this study, the CHO-MG cell line represents cells with no PAT activity and provided a model for alternative modes of entry or action that are independent of PAT. These alternative modes of entry include passive diffusion or utilization of another transporter. The alternative modes of action may also include interactions on the outer surface of the plasma membrane or other membrane receptor interactions.

In contrast, the parent CHO cell line represents a cell type with high PAT activity.⁸ Comparison of conjugate cytotoxicity in these two CHO lines provided an important screen to detect selective conjugate delivery via the PAT. For example, a conjugate with high utilization of the polyamine transporter would be very toxic to CHO cells, but less so to CHO-MG cells.⁸ In short, highly selective PAT ligands should give high CHO-MG/CHO IC₅₀ ratios.

None of the norspermidines (**4a**, **6a**, and **7a**) were PAT-selective and each had a CHO-MG/CHO IC₅₀ ratio near 1 (Table 1).³ In this regard, the *N*¹-ethyl-*N*¹-anthracenylmethyl derivatives

(**7a,b**) further mirrored the bioactivity of the dihydromotuporamines (**4a,b**).

The norspermidine derivatives **4a** and **7a** were consistently more toxic (e.g., 2.8–10-fold) than their homospermidine counterparts, **4b** and **7b**, in the tested cell lines. Moreover, incremental changes in the polyamine motifs of **4** (i.e., **4a** vs **4b**) gave the same relative cytotoxicity trend as observed with **7a** and **7b**, respectively. Interestingly, this trend in the relative IC₅₀ and K_i values observed with **4a** and **4b** (Table 1) was also observed with the *N*-ethylated derivatives **7a** and **7b**, but not for the nonethylated derivatives **6a** and **6b**. These observations suggested that *N*¹-ethylated systems (e.g., **7a**) may be good dihydromotuporamine mimics.

These homologues also provided insight into PAT selectivity. For example, *N*¹-ethyl derivative **7b** gave no PAT selectivity. In contrast, the nonethylated system **6b** had 148-fold higher toxicity in the CHO cell line due to its use of the polyamine transporter for cellular entry.⁸ Clearly, the introduction of an additional ethyl group at the *N*¹ position dramatically altered the biological profile of these related systems (**6** and **7**).⁸ Therefore, a molecular modeling study was initiated, to better understand the potential molecular shapes involved in dihydromotuporamine mimicry (e.g., **4a** vs **7a**) and in PAT recognition (e.g., **6b** vs **7b**).

Molecular Modeling. The triamine centers were protonated for modeling purposes, since spermidine exists predominantly as the trication at physiological pH.¹⁵ Not surprisingly, the polyamine chains typically prefer the anti-conformer all along the methylene chain spacer (e.g., N–(CH₂)_{*n*}–N), regardless of the length of this spacer. Therefore, the first challenge was to model the macrocycles present in the motuporamine systems **1**–**4**.

Andersen and co-workers have previously outlined a naming methodology to report the conformations of the macrocycles present in the motuporamine family.^{2a} A particular conformer can be described by listing the number of contiguous bonds, which are anti. These “anti spacers” separate the gauche “turn centers”. To form a ring, a completely anti system is impossible, because no “turn” or curvature is introduced to close the ring. To cyclize, some methylene centers must orient their neighboring carbon atoms in a gauche conformation. (Note: in terms of

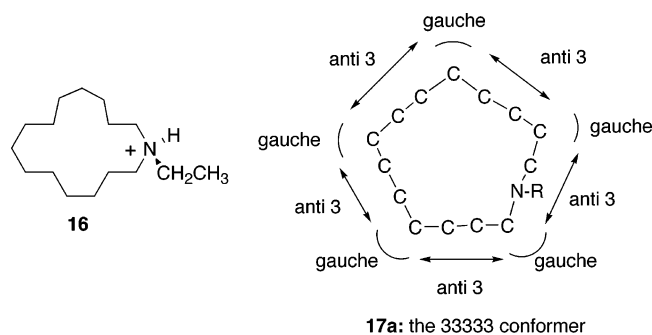


Figure 3. Model **16** and its conformer **17a**.

anti and gauche, we are referring to the C–C–C–C dihedral angle. When nitrogen is involved, one of the C's is then replaced by nitrogen, e.g., C–C–N–C.) This essentially turns the chain back toward itself and with the proper number of “gauche turns” allows ring formation. Using this insight, one can define the spatial arrangement of a particular conformer by listing the number of contiguous bonds that are anti and separate the gauche “turn centers”.

As shown in Figure 3, the nitrogen is involved in an array of dihedrals (e.g., C–C–N–C) that can be classified as anti. The conformer designation starts by counting the number of bonds within the string of anti dihedrals containing the lone nitrogen center. In this example, there are three bonds near (or including) the nitrogen atom that have successive anti conformations (designated as “anti 3”, Figure 3). The next dihedral is gauche (and begins the necessary turn) as one continues clockwise around the 15-membered ring. This in turn leads to another string of three bonds containing anti dihedrals, which terminates

in a gauche dihedral. This sequence occurs three more times and terminates in the final gauche turn, which closes the ring system. Therefore, one conformer of **16** is referred to as a 33333 conformer (**17a**, Figure 3).¹

The same approach was used throughout the modeling studies with **1–4**. For brevity, the modeling of **4a** will be described as an example.

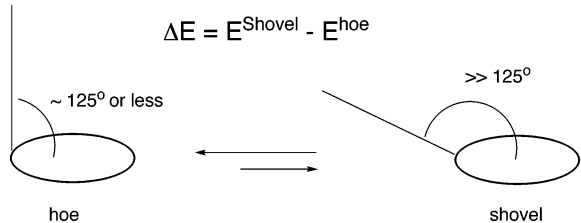
Dihydratotuporamine C (**4a**) was first modeled as its *N*-ethyl heterocycle **16** (Figure 3). Using the MMFF molecular mechanics program from PC Spartan*pro* (Wavefunction, Inc.), model **16** was constructed and geometry-optimized by several algorithms.

Model **16** was first subjected to conformational analysis using the Monte Carlo stochastic search program supplemented with a geometry-optimizing MMFF force field and gave 2403 conformers. The most stable 50 conformers were selected and subjected to semiempirical PM3 geometry optimization. The most stable 20 of these conformers were subjected to Hartree–Fock/STO-3G geometry optimization. From these, the most stable nine conformers were selected for further optimization at the HF/3-21G(d) level of computation. The difference in energy between the most and least stable conformers (ΔE) of the nine conformers was 5.17 kcal/mol. The five lowest energy conformers were selected and imported into the GaussView program (Gaussian 98). Next, the necessary polyamine fragment was added to complete the 3,3-triamine sequence in **4a**. The fully assembled **4a** was then geometry-optimized at the HF/3-21G(d) level. Each of the five conformers gave a lowest energy form, which is listed in Table 2. [Note: the conformer designation (e.g. 33333) refers to the previously mentioned ring nomenclature.]

Table 2. Relative Energies and Shapes of the Most Stable Conformers of **4a**

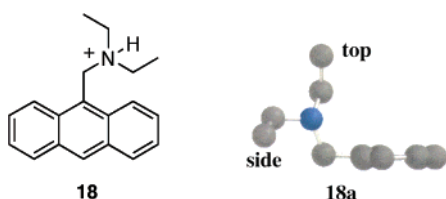
Shape:	hoe	hoe	shovel	hoe	shovel
Designation:	<u>33333N2</u> ^b	<u>23424</u>	<u>33333N1</u> ^b	<u>24234</u>	<u>23424</u>
Side View ^a					
Front View ^a					
Top View ^a					
Relative energy: (Kcal/mol)	0.00	0.27	0.94	1.15	1.34

^a View shown relative to the polyamine chain and not the ring. ^b Position of nitrogen in pentagonal segment is different. 33333N2 and 33333N1 have the nitrogen either at the nonapex or apex position of their pentagon, respectively.

Table 3. Relative Energies and Geometries Associated with the Hoe and Shovel Shapes of 4–7^a


compd	rel energy (ΔE , kcal/mol) ^b	approx angle of tether and ring plane (deg)	
		hoe	shovel
4a	0.94	123	155
4b	0.78	125	154
5	3.22	97	139
6a	0.72	90	139
6b	0.08	92	139
6c	5.68	109	139
7a	2.89	NM ^c	165
7b	1.00	82	165

^a In all cases the hoe conformer was the lowest energy form. ^b ΔE represents the energy difference between the lowest energy shovel conformer and the lowest energy conformer found (hoe). ^c NM: not meaningful; see the Supporting Information for images of **7a**.

**Figure 4.** Diethyl model **18** and its lowest energy conformer, **18a**.

As shown in Table 2, the aliphatic ring in **4a** is conformationally mobile. Surprisingly, three of the five lowest energy conformers resemble an overall “hoe” shape, where the appended polyamine chain is oriented vertically over the ring. This approach provided insight into the geometric preferences of the 15-membered heterocycle and its preferred orientation relative to the appended polyamine.

Indeed, other modeling experiments indicated that all of the aliphatic 13-, 14-, and 15-membered macrocycles seemed to prefer a “relatively” flat shape similar to anthracene. A similar finding was made by Andersen et al. in their comparison of **4a** and carbazole **5**.^{2a} The preferred conformers found by this approach for **1–3**, **4b**, **5–7** are provided in the Supporting Information.

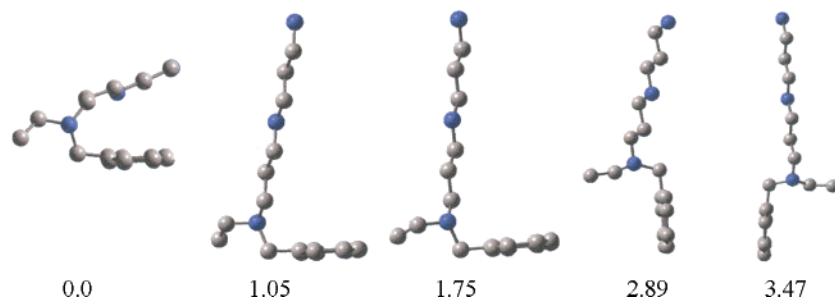
Compounds **1–3**, **4a**, **5**, **6a**, and **7a** have 3,3-triamine sequences, while **4b**, **6b–d**, and **7b** have 4,4-triamine sequences. Their respective “all-anti” polyamine chains are oriented along a line and represent a straight “shaft” extending from the relatively flat macrocycle or anthracene ring system. The key features, therefore, are the relative orientation of the shaft with respect to the “plane” of the macrocycle. These differences are illustrated as “hoe” and “shovel” shapes in Tables 2 and 3.

To compare the shapes of the motuporamine analogues to the anthracene systems, molecule **18** was constructed and geometry-optimized by the above procedure to give the lowest energy conformer shown in Figure 4.

The *N*-ethylated derivatives **7a** and **7b** were constructed from this optimized conformer **18a**. For example, **7a** was constructed by first transferring **18a** to GaussView and appending the appropriate polyamine architecture onto either position shown in Figure 4 (“top” or “side”) to generate two conformers of **7a** with the 3,3-triamine sequence either oriented vertically (using top) or sideways (using the side ethyl group position). These two conformers were then geometry-optimized using the 3-21G(d) level of computation. To further sample the potential-energy landscape, the next three higher energy conformers found with **18** were also structurally converted to **7a** in GaussView and geometry-optimized using the 3-21G(d) level of computation. This provided a series of conformers, which were ranked according to their relative energies (Figure 5).

It should be noted that the three lowest energy conformers each had the polyamine chain vertically oriented over the ring system (hoe shape) regardless of whether they were originally built from the top or side ethyl group position! As shown in Figure 5, the lowest energy shovel-shaped conformer found was 2.89 kcal/mol higher in energy than the lowest energy hoe conformer.

Indeed, there seemed to be a distinct preference for both the *N*-ethylated systems (**7a,b**) to orient the polyamine chain over the anthracene ring. In short, the hoe motif seemed to be energetically preferred in both the dihydromotuporamine and

**Figure 5.** Most stable conformers found with **7a** (relative energies listed in kcal/mol).

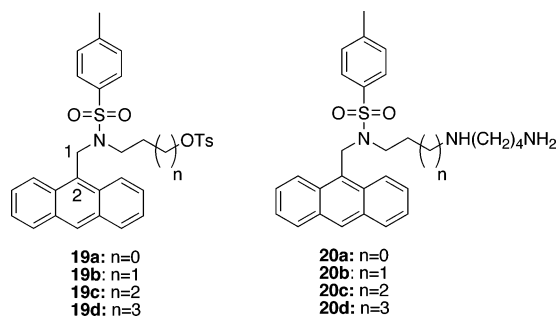


Figure 6. Other analogues **19** and **20**.

N-ethylated anthracene systems (see Tables 2 and 3 and Supporting Information).

It should be noted that this type of cation– π interaction (observed with **7**) is common in protein architectures containing amino acids with aromatic and cationic side chains. In fact, Gallivan and Dougherty in their survey of cation– π interactions in the Protein Data Bank concluded that “when a cationic side chain is near an aromatic side chain, the geometry is biased toward one that would experience a favorable cation– π interaction”.¹⁷

Inspection of the lowest energy conformers of these systems provided a possible explanation for the different bioactivities observed with **4**–**7**. In short, there is a significant shape preference associated with the presence of the *N*¹-tertiary amine center. For example, as shown in Table 3, the energy differences for the lowest energy shovel conformer and the overall lowest energy conformer (hoe) of PAT-selective **6b** is minimal ($\Delta E = E_{\text{shovel}} - E_{\text{hoe}} = 0.08$ kcal/mol) in comparison to (non-PAT selective) *N*-ethylated **7b** ($\Delta E = 1.00$ kcal/mol). The difference is large in the other paired systems as well (ΔE for **6a**, 0.72; **7a**, 2.89 kcal/mol). The carbazole **5** has $\Delta E = 3.22$ kcal/mol. While *E* does not describe the activation barrier for interconversion between these two forms (hoe and shovel), it does reveal the thermodynamic preference for adopting the hoe shape in the non-PAT selective ligands.

It is interesting to note that **4a,b** and **7a,b** all contain tertiary amine centers at the *N*¹-position, prefer the hoe shape, and have no PAT selectivity (Table 1).³ Clearly, *N*¹-ethylation (**7b**) obliterated the PAT selectivity of **6b**.³ Although speculative, the data also suggests that a shovel motif may play a role in the high selectivity of **6b** for the polyamine transporter.

It is important to note that molecular shape is not the only parameter that facilitates cellular entry. While **6a** can also adopt the shovel shape for possible PAT recognition, **6a** is not a PAT-selective ligand due to its 3,3-triamine sequence.⁵ This norspermidine (3,3-triamine) sequence represents a discreet separation of protonated nitrogen centers at physiological pH and has been shown to be a poor ligand for the PAT.⁵ This observation is consistent with the previously discussed, PAT-ligand structural requirements.^{5,8} Although the norspermidine derivatives (**4a**, **6a**, and **7a**) do not enter cells via the polyamine transporter (Table 1), they do gain entry to cells by other means.

Therefore, it is plausible that access to the shovel conformer (and having the homospermidine motif) facilitates PAT use (e.g., **6b**), while the hoe shape and having the norspermidine motif facilitates dihydromotoporamine C mimicry (e.g., **7a**).

Crystal Structures. It is important to realize that the computed structures above were performed *in silico*. The preferred conformations in solution and the solid state may be quite different.

Prior studies revealed a similar conformational constraint introduced by having two bulky *N*¹-substituents in *N*¹-anthracen-

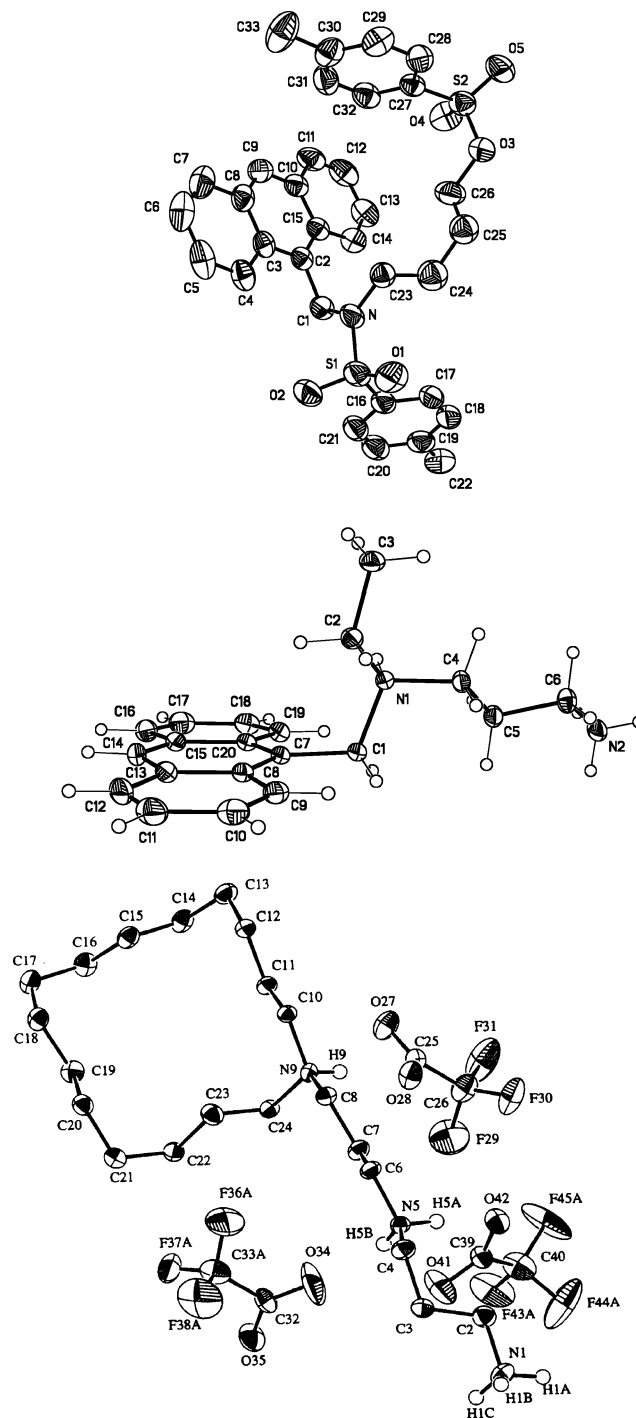


Figure 7. ORTEP drawings of **19c** (top, ref 13), **12d** (middle), and **4c** (bottom, TFA salt, from ref 2a).

9-ylmethyl-*N*¹-tosyl-polyamine systems **19** and **20** (Figure 6).¹³ A single crystal of **19c** revealed that the longer *N*-alkyl chain was oriented over the anthracene ring system (top, Figure 7). This effect was rationalized by the anti alignment imparted by the C2–C1–N–S1 dihedral angle, presumably due to steric effects associated with the *N*¹-sulfonamide group (Figure 7).¹³ In addition, prior ¹H NMR studies (in CDCl₃) with **19** and **20** revealed a persistent *upfield* shift in the respective polyamine chain chemical shifts (presumably due to shielding effects of the anthracene π system).¹³ In short, *N*¹-sulfonylation introduced a conformational constraint on the appended *N*-alkyl chain, which preferentially oriented the polyamine over the anthracene ring system.¹³

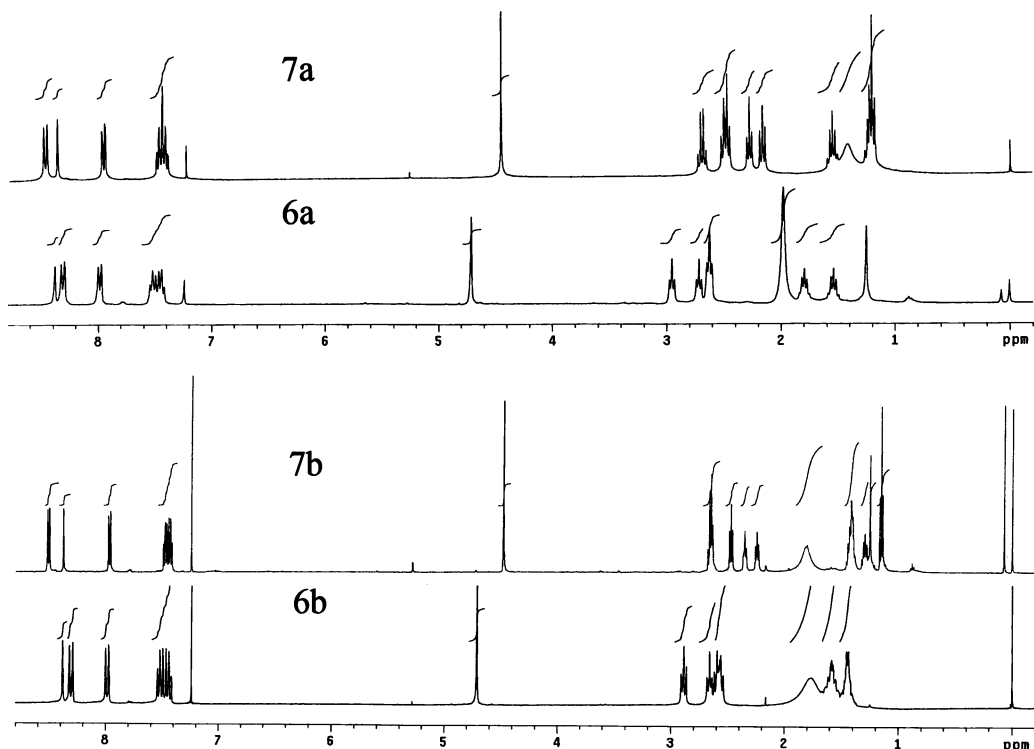


Figure 8. ^1H NMR spectra of the free amines of the norspermidines (**6a**, **7a**) and homospermidines (**6b**, **7b**) in CDCl_3 .

Likewise, a single crystal of **12d** (middle, Figure 7) indicated that the more bulky, longer alkyl chain was preferentially oriented away from the anthracene ring, while the smaller *N*-ethyl chain was oriented over the anthracene ring. In addition, Andersen et al. have reported a crystal structure of a 16-membered dihydromotuporamine analogue (**4c**, trifluoroacetic acid salt; Figures 1 and 7) that adopted similar dihedral angles as **12d** in the solid state.^{2a} Using the respective atom assignments shown in Figure 7, the dihedral angle C7–C1–N1–C4 for **12d** was 180° and the angle C11–C10–N9–C8 for **4c** was 178.5° .^{2a} These dihedral angles and the anti orientation of the respective, appended polyamine chains generate an overall shovel motif for both **12d** and **4c**. Therefore, **19c**, **12d**, and **4c** all revealed that in the solid state, the bulkiest *N*¹-substituent is oriented away from the large anthracene (or aliphatic) ring system. Moreover, the *N*⁹ and *N*¹ positions (as denoted in Figure 7) had similar dihedral angles and relative orientations of their *N*-alkyl substituents for both **4c** and **12d**, respectively.

Initially, the solid-state preferences found with **12d** seemed to contradict the aforementioned modeling results, which suggested that the polyamine chain (and not the *N*-ethyl group) was oriented toward the anthracene ring system, especially for the related 3,3-triamine system, **7a**. Since the crystal packing of **12d** revealed only solid-state preferences, ^1H NMR studies were needed to better describe the preferred solution structure of these *N*-ethyl systems (**7a,b** and **12d**).

The appended anthracene ring and its known shielding properties were used to solve this dilemma by considering two cases.

Case 1. If the crystal structure of **12d** was the best predictor of the solution structure of **7a**, then the polyamine would be oriented away from the π system of the anthracene ring and would be relatively ‘immune’ to its shielding effects. Ideally, one would expect to see no dramatic upfield shifts for the polyamine’s methylene groups in this case.

Case 2. If the modeling work was a good indicator of the solution structure of **7a**, then the polyamine would be oriented

over the anthracene ring (e.g., ‘hoe’ structure) and one would expect to see dramatic shielding effects such as those noted earlier with **19** and **20**. In this case, the rotamer, which orients the polyamine over the ring π system, would be a significant contributor to the preferred solution structure.

^1H NMR Studies. Rewardingly, ^1H NMR studies (in CDCl_3) of the free amines of the related analogues (**7a,b** and **12–14**) revealed a significant shielding effect for these *N*-ethylated derivatives and not for the derivatives **6a,b** (sans ethyl). These observations clearly support case 2 and are provided in the Supporting Information.

Typically, conversion of a secondary amine (e.g., dipentylamine) to a tertiary amine (e.g., tripentylamine) results in a δ 0.2 upfield shift of the adjacent $(\text{RCH}_2)_3\text{N}$ protons.¹⁶ A comparison of the ^1H NMR spectra of the free amines of **6a** and **7a** (and **6b** and **7b**) revealed the expected 0.2 ppm upfield shift of the benzylic hydrogens upon formation of the new *N*¹-tertiary center (Figure 8). However, significant upfield shifts in the other NCH_2 groups were also observed, especially those that are quite distal to the new *N*-Et center. These spectral changes are far beyond those expected for simple tertiary amine formation at the *N*¹-position.¹⁶

As shown in Figure 8, the ^1H NMR spectra (in CDCl_3) of the free amine systems of **6a** and **6b** typically give a cluster of CH_2N signals between δ 2.55 and 2.95. In the *N*¹-ethylated derivatives (i.e., **7a,b**), many of these signals are shifted significantly upfield, presumably due to their closer proximity to the anthracene shielding cone. Upon *N*¹-ethylation, changes occur in the aromatic region of the spectra (doublet at 8.3 moves downfield to $\sim\delta$ 8.45) as well, indicating a possible interaction between the anthracene and polyamine components of the conjugate. Using ^1H – ^1H COSY NMR experiments, we were able to assign the chemical shifts of these systems, and these are listed in the Supporting Information. Examples of the ^1H NMR spectra of **6a**, **7a** and **6b**, **7b** are given in Figure 8.

The fact that the nonethylated uncharged amines of **6a** do not show this polyamine shielding effect (Supporting Informa-

tion) implies that the additional N^1 -ethyl group (3° amine formation) imparts the conformational constraint or preference. Indeed, this N^1 -substitution trend holds true for a variety of N -ethylated anthracenylmethyl model systems **12**–**14** (see Supporting Information). These other systems are spectrally less complex, and the trend is readily observed. While this effect is somewhat muted in the hydrochloride forms of **6** and **7**, it is still apparent in D_2O for the HCl salts of **6a** vs **7a**.

Since the shielding effect should be sensitive to distance, the large shielding observed is consistent with close contact between the polyamine chain and the anthracene π system. These observations (coupled with our earlier investigations of the behavior of **19** and **20**) allowed us to conclude that the hoe motif is a major contributor to the solution structure of the free amine of **7a**, especially in hydrophobic environments such as $CDCl_3$. This shielding effect was also shown to be independent of polyamine conjugate concentration over the range studied (100–1 mM free amine **7a** in $CDCl_3$). This latter observation further supported an intramolecular effect and the putative hoe shape for **7a**.

It should be mentioned that the interactions of free amine systems with aromatic π systems are quite rare, whereas the related cation– π interactions of ammonium salts and aromatic ring systems are better documented in the literature.¹⁷ As such, these simple N -anthracen-9-ylmethyl, N -ethyl architectures may provide new tools to study these novel types of interactions in both the free amine and ammonium ion states.

In summary, the 1H NMR studies supported a hoe shape for the free amine of **7a** and suggested that a tertiary amine motif at the N^1 -position imparts a conformational preference that orients the polyamine over the adjacent ring system.

Conclusions

Although the actual conformations of the modeled systems may be significantly different than those proposed in this report, our results suggest that N^1 -ethylation, to form a 3° amine at the N^1 -position, imparts a conformational preference (e.g., hoe), especially in norspermidine derivatives (i.e., 3,3-triamines).

These insights offer another possible explanation for the loss of PAT selectivity upon N^1 -ethylation of **6b** beyond those previously mentioned.³ The modeling results and 1H NMR spectral changes observed with **6b** suggested that a “shovel” motif could be preferred by this PAT-selective conjugate, while the “hoe” shape induced by the N^1 -tertiary center in **7b** is likely not processed by the polyamine transporter (see Table 1). In addition, the extended N^1 -alkyl tether systems **6c** and **6d** (Figure 1) also preferred the hoe shape and were also less efficient PAT ligands⁸ (see Supporting Information).

Our findings suggested that “hoe-shaped” norspermidine analogues may be excellent dihydromotuporamine C (**4a**) mimics. The observations that **4a** and **7a** have similar shape preferences and initial biological activities (e.g., L1210 cytotoxicity and CHO-MG/CHO IC₅₀ ratio) supported this premise.

In summary, the degree of substitution at the N^1 -position seems to be an important determinant of both the molecular shape preferences and biological activity of these anthracenylmethyl polyamine conjugates. Such insights will be of great assistance to medicinal chemists interested in designing PAT-selective ligands as well as future dihydromotuporamine C mimics.

Experimental Section

Materials. Silica gel (32–63 μm) and chemical reagents were purchased from commercial sources and used without further purification. All solvents were distilled prior to use. Reactions were

carried out under a nitrogen atmosphere. 1H and ^{13}C spectra were recorded at 300 or 75 MHz, respectively. TLC solvent systems are listed as volume percents, and NH_4OH refers to concentrated aqueous NH_4OH . All tested compounds provided satisfactory elemental analyses (see Supporting Information).

Biological Evaluation Methods. The methods were identical to those described previously in ref 3.

N -(3-Aminopropyl)- N' -anthracen-9-ylmethyl- N' -ethylpropane-1,3-diamine, Hydrochloride Salt (7a**).** A solution of Boc-protected **11** (700 mg, 1.28 mmol) was dissolved in absolute ethanol (13 mL) and stirred at 0 °C for 10 min. A 4 N HCl solution (22 mL) was added to the reaction mixture dropwise and stirred at 0 °C for 20 min and then at room temperature overnight. The solution was concentrated in vacuo to give **7a** as a yellow solid in 90% yield: 1H NMR (D_2O) δ 8.23 (s, 1H), 7.91 (m, 4H), 7.70 (m, 2H), 7.59 (m, 2H), 4.70 (s, 2H), 3.34 (m, 2H), 3.11 (m, 4H), 3.00 (t, 2H), 2.84 (t, 2H), 2.05 (q, 2H), 1.96 (m, 2H), 1.41 (m, 3H); ^{13}C NMR (D_2O) δ 133.7, 133.1 (3C), 132.3 (2C), 130.7 (2C), 128.1 (2C), 125.0 (2C), 121.1 (2C), 52.1, 51.8, 47.3, 47.2, 39.3 (2C), 26.5, 23.5, 11.32; HRMS (FAB) calcd for $C_{23}H_{31}N_3 \cdot 3HCl$ (M + H – 3HCl)⁺ 350.2591, found 350.2588.

{3-[(Anthracen-9-ylmethyl)amino]propyl}(3-*tert*-butoxycarbonylamino)propyl}carbamic Acid *tert*-Butyl Ester (10**).** To a stirred solution of amine **9** (1 g, 3.02 mmol) in 25% MeOH/ CH_2Cl_2 (20 mL) was added a solution of 9-anthraldehyde **8** (0.519 g, 2.52 mmol) in 25% MeOH/ CH_2Cl_2 (15 mL) under N_2 . The mixture was stirred at room temperature overnight until the imine formation was complete (monitored by NMR). The solvent was removed in vacuo, the solid residue dissolved in 50% MeOH/ CH_2Cl_2 (40 mL), and the solution cooled to 0 °C. $NaBH_4$ (7.55 mmol) was added in small portions to the solution and the mixture was stirred at room temperature overnight. The solvent was removed in vacuo and the solid residue dissolved in CH_2Cl_2 (40 mL) and washed with Na_2CO_3 solution (10% aq, 3 \times 30 mL). The CH_2Cl_2 layer was dried over anhydrous Na_2SO_4 and filtered, and the solvent was removed in vacuo to give an oily residue. The oil was purified by flash column chromatography (5% MeOH/ $CHCl_3$) to yield the product **10** as a pale yellow thick oil (0.38 g, 75%): R_f = 0.3 (5% MeOH/ $CHCl_3$); 1H NMR ($CDCl_3$) δ 8.39 (s, 1H), 8.34 (d, 2H), 7.99 (d, 2H), 7.53 (m, 2H), 7.46 (m, 2H), 4.70 (s, 2H), 3.18–3.24 (m, 4H), 3.06 (br t, 2H), 2.85 (br t, 2H), 1.77 (br q, 2H), 1.60 (br q, 2H), 1.44 (m, 18H); ^{13}C NMR ($CDCl_3$) δ 156.1 (2C), 131.6, 130.3 (2C), 129.2 (2C), 127.2 (2C), 126.1 (2C), 125.0 (3C), 124.2 (2C), 79.7 (2C), 53.7, 48.0, 46.0, 45.3, 44.0, 37.6, 29.6, 28.7 (6C), 27.5; HRMS (FAB) m/z calcd for $C_{31}H_{43}N_3O_4$ (M + H)⁺ 522.3326, found 522.3304.

{3-[(Anthracen-9-ylmethylethylamino)propyl](3-*tert*-butoxycarbonylamino)propyl}carbamic Acid *tert*-Butyl Ester (11**).** Ethyl bromide (EtBr, 508 mg, 4.66 mmol) was dissolved in anhydrous acetonitrile and added to a stirring mixture of compound **10** (805 mg, 1.55 mmol) and anhydrous K_2CO_3 (644 mg, 4.66 mmol). The mixture was then stirred overnight at 75 °C under a N_2 atmosphere. After confirmation of the disappearance of **10** by TLC, the solution was concentrated under reduced pressure. The residue was dissolved in CH_2Cl_2 (20 mL) and washed three times with aqueous sodium carbonate. The organic layer was separated, dried with anhydrous Na_2SO_4 , filtered, and concentrated under vacuum. Flash column chromatography of the residue gave **11** as a light yellow oil: yield 80%; R_f = 0.35 (3% MeOH/ $CHCl_3$); 1H NMR ($CDCl_3$) δ 8.43 (d, 2H), 8.25 (s, 1H), 7.86 (d, 2H), 7.43 (m, 2H), 7.37 (m, 2H), 4.34 (s, 2H), 2.78–2.92 (m, 4H), 2.64 (m, 4H), 2.36 (m, 2H), 1.21–1.48 (m, 23H), 1.16 (m, 2H); ^{13}C NMR ($CDCl_3$) δ 155.7, 131.1 (3C), 131.0, 128.7 (2C), 127.0 (2C), 125.2 (2C), 124.8 (2C), 124.5 (2C), 78.9, 78.4, 53.4, 50.6, 50.0, 47.9, 45.3, 43.5, 37.1, 28.3 (6C), 26.5, 11.7; HRMS (FAB) m/z calcd for $C_{33}H_{47}N_3O_4$ (M + H)⁺ 550.3639, found 550.3619.

{3-[(Anthracen-9-ylmethyl)amino]propyl}carbamic Acid *tert*-Butyl Ester (12a**).** To a stirred solution of mono-Boc-protected 1,3-diamine **15b** (1 g, 5.75 mmol)^{14a,c} in 25% MeOH/ CH_2Cl_2 (20 mL) was added a solution of 9-anthraldehyde **8** (0.99 g, 4.8 mmol) in 25% MeOH/ CH_2Cl_2 (15 mL) under N_2 . The mixture was stirred

at room temperature overnight until the imine formation was complete (monitored by NMR). The solvent was removed in vacuo, the solid residue dissolved in 50% MeOH/CH₂Cl₂ (40 mL), and the solution cooled to 0 °C. NaBH₄ (14.42 mmol) was added in small portions to the solution and the mixture was stirred at room temperature overnight. The solvent was removed in vacuo, and the solid residue was dissolved in CH₂Cl₂ (40 mL) and washed with Na₂CO₃ solution (10% aq, 3 × 30 mL). The CH₂Cl₂ layer was dried over anhydrous Na₂SO₄ and filtered, and the solvent was removed in vacuo to give an oily residue. The oil was purified by flash column chromatography (5% MeOH/CHCl₃) to yield the product **12a** as a pale-yellow, thick oil (75%): *R*_f = 0.3 (5% MeOH/CHCl₃); ¹H NMR (CDCl₃) δ 8.20 (m, 3H), 7.85 (d, 2H), 7.43 (m, 2H), 7.36 (m, 2H), 5.32 (t, 1H), 4.52 (s, 2H), 3.10 (q, 2H), 2.77 (t, 2H), 1.56 (q, 2H), 1.39 (s, 9H); ¹³C NMR (CDCl₃) δ 156.0, 131.3 (2C), 130.1 (2C), 129.0 (2C), 127.0 (2C), 125.9 (2C), 124.8 (2C), 124.0 (2C), 78.7 (2C), 48.5, 45.8, 39.4, 29.9, 28.5; HRMS (FAB) *m/z* calcd for C₂₃H₂₈N₂O₂ (M + H)⁺ 365.2224, found 365.2208.

N¹-Anthracen-9-ylmethylpropane-1,3-diamine, Hydrochloride Salt (12b). A solution of **12a** (200 mg, 0.51 mmol) was dissolved in absolute ethanol (6 mL) and stirred at 0 °C for 10 min. A 4 N HCl solution (10 mL) was added to the reaction mixture dropwise and stirred at 0 °C for 20 min and then at room temperature overnight. The solution was concentrated in vacuo to give **12b** as a yellow solid in 90% yield: ¹H NMR (CD₃OD) δ 8.69 (s, 1H), 8.39 (d, 2H), 8.15 (d, 2H), 7.74 (m, 2H), 7.60 (m, 2H), 5.33 (s, 2H), 3.45 (t, 2H), 3.12 (t, 2H), 2.23 (q, 4H); ¹³C NMR (CD₃OD) δ 132.6, 132.0, 131.6, 130.6, 129.0, 126.7, 124.0, 122.5, 46.6, 44.6, 38.1, 25.4; HRMS (FAB) calcd for C₁₈H₂₀N₂·2HCl (M + H - 2HCl)⁺ 265.1699, found 265.1704.

[3-(Anthracen-9-ylmethyl ethylamino)propyl]carbamic Acid tert-Butyl Ester (12c). Bromoethane (489 mg, 4.48 mmol) was dissolved in anhydrous acetonitrile and added to the stirring mixture of compound **12a** (545 mg, 1.5 mmol) and anhydrous K₂CO₃ (620 mg, 4.48 mmol). The mixture was then stirred at 75 °C under a N₂ atmosphere overnight. After confirmation of the disappearance of **12a** by TLC, the solution was concentrated under reduced pressure. The residue was dissolved in CH₂Cl₂ (20 mL) and washed three times with aqueous sodium carbonate. The organic layer was separated, dried with anhydrous Na₂SO₄, filtered, and concentrated under vacuum. Flash column chromatography of the residue gave **12c** as a light yellow oil: yield 80%; *R*_f = 0.35 (3% MeOH/CHCl₃); ¹H NMR (CDCl₃) δ 8.39 (d, 2H), 8.30 (s, 1H), 7.90 (d, 2H), 7.40 (m, 4H), 4.54 (br t, 1H), 4.37 (s, 2H), 2.74 (q, 2H), 2.60 (q, 2H), 2.39 (t, 2H), 1.44 (q, 2H), 1.31 (m, 9H), 1.12 (t, 3H); ¹³C NMR (CDCl₃) δ 155.7, 131.3 (2C), 131.2 (2C), 130.4 (2C), 129.0 (2C), 127.5 (2C), 125.7 (2C), 124.8 (2C), 78.3, 50.6, 50.5, 47.7, 39.1, 28.6 (3C), 26.6, 11.8; HRMS (FAB) *m/z* calcd for C₂₅H₃₂N₂O₂ (M + H)⁺ 393.2537, found 393.2523.

N¹-Anthracen-9-ylmethyl-N¹-ethylpropane-1,3-diamine, Hydrochloride Salt (12d). A solution of **12c** (400 mg, 1.02 mmol) was dissolved in absolute ethanol (13 mL) and stirred at 0 °C for 10 min. A 4 N HCl solution (22 mL) was added to the reaction mixture dropwise and stirred at 0 °C for 20 min and then at room temperature overnight. The solution was concentrated in vacuo to give **12d** as a yellow solid in 90% yield: ¹H NMR (D₂O) δ 8.42 (s, 1H), 8.0 (m, 4H), 7.71 (m, 2H), 7.61 (m, 2H), 4.87 (s, 2H), 3.34 (br q, 2H), 3.14 (br t, 2H), 2.81 (t, 2H), 2.00 (q, 2H), 1.40 (t, 3H); ¹³C NMR (D₂O) δ 133.8, 133.3 (3C), 132.4 (2C), 130.7 (2C), 128.2 (2C), 125.1 (2C), 121.5 (2C), 52.0, 51.9, 39.2 (2C), 24.5, 11.3; HRMS (FAB) calcd for C₂₀H₂₄N₂·2HCl (M + H - 2HCl)⁺ 293.2012, found 293.2009.

3-[(Anthracen-9-ylmethyl)amino]propan-1-ol, 14a.⁵ To a stirred solution of 3-amino-1-propanol (**15a**) (0.87 g, 11.65 mmol) in 25% MeOH/CH₂Cl₂ (20 mL) was added a solution of aldehyde **8** (2.00 g, 9.7 mmol) in 25% MeOH/CH₂Cl₂ (15 mL) under N₂. The mixture was stirred at room temperature overnight until the imine formation was complete (monitored by NMR). The solvent was removed in vacuo, the solid residue dissolved in 50% MeOH/CH₂Cl₂ (40 mL), and the solution was cooled to 0 °C. NaBH₄ (29.1 mmol) was added in small portions to the solution and the mixture was stirred at room

temperature overnight. The solvent was removed in vacuo, and the solid residue was dissolved in CH₂Cl₂ (40 mL) and washed with 10% aq Na₂CO₃ solution (3 × 30 mL). The CH₂Cl₂ layer was separated, dried over anhydrous Na₂SO₄, filtered, and concentrated in vacuo to give an oily residue. The oil was purified by flash column chromatography (6% MeOH/CHCl₃) to yield the product **14a**⁵ as a pale yellow thick oil (78%): *R*_f = 0.3 (6% MeOH/CHCl₃); ¹H NMR (CDCl₃) δ 8.39 (s, 1H), 8.27 (d, 2H), 7.99 (d, 2H), 7.52 (m, 2H), 7.45 (m, 2H), 4.71 (s, 2H), 3.79 (t, 2H), 3.09 (t, 2H), 1.74 (q, 2H).

3-(Anthracen-9-ylmethyl ethylamino)propan-1-ol, 14b. Bromoethane (616 mg, 5.65 mmol) was dissolved in anhydrous acetonitrile and was added to the stirring mixture of compound **14a**⁵ (500 mg, 1.9 mmol) and anhydrous K₂CO₃ (781 mg, 5.7 mmol). The mixture was then stirred overnight at 75 °C under a N₂ atmosphere. After confirmation of the disappearance of **14a** by TLC, the solution was concentrated under reduced pressure. The residue was dissolved in CH₂Cl₂ (20 mL) and washed three times with aqueous sodium carbonate. The organic layer was separated, dried with anhydrous Na₂SO₄, filtered, and concentrated under vacuum. Flash column chromatography of the residue gave **14b** as a light yellow oil: yield 82%; *R*_f = 0.35 (3% MeOH/CHCl₃); ¹H NMR (CDCl₃) δ 8.28 (m, 3H), 7.86 (d, 2H), 7.44 (m, 2H), 7.36 (m, 2H), 4.29 (s, 2H), 3.15 (t, 2H), 2.65 (q, 2H), 2.52 (t, 2H), 1.43 (q, 2H), 1.16 (t, 3H); ¹³C NMR (CDCl₃) δ 131.2, 131.1, 129.3, 129.0, 127.6, 125.8, 124.8, 124.4, 63.4, 52.6, 50.5, 47.7, 28.1, 11.6; HRMS (FAB) *m/z* calcd for C₂₀H₂₃NO (M + H)⁺ 294.1852, found 294.1859.

X-ray Experimental. Data were collected at 173 K on a Siemens SMART PLATFORM equipped with a CCD area detector and a graphite monochromator utilizing Mo Kα radiation (λ = 0.710 73 Å). Cell parameters were refined using up to 8192 reflections. A full sphere of data (1850 frames) was collected using the ω-scan method (0.3° frame width). The first 50 frames were remeasured at the end of data collection to monitor instrument and crystal stability (maximum correction on *I* was < 1%). Absorption corrections by integration were applied on the basis of measured indexed crystal faces.

The structure was solved by the Direct Methods in *SHELXTL6* (2000) by Bruker-AXS (Madison, WI) and refined using full-matrix least squares. The non-H atoms were treated anisotropically, whereas the hydrogen atoms were calculated in ideal positions and were riding on their respective carbon atoms. The asymmetric unit consists of the dication, two chloride anions, and a water molecule of crystallization. All acidic protons, those on both N atoms and water, are involved in H bonding. A total of 251 parameters were refined in the final cycle of refinement using 11 952 reflections with *I* > 2σ(*I*) to yield R1 and wR2 of 2.95% and 8.52%, respectively. Refinement was done using *F*².

Acknowledgment. O.P. thanks Dr. David Powell at the University of Florida mass spectrometry facility for his kind assistance in acquiring the mass spectra of these compounds. O.P. acknowledges both the Florida Hospital Endowed Program for Oncological Research and, in part, the Broad Medical Research Program of the Eli and Edythe L. Broad Foundation for their support of this research and the University of Central Florida Office of Research and Commercialization for funding the acquisition of a new NMR probe. K.A.A. acknowledges the National Science Foundation and the University of Florida for funding of the purchase of the X-ray equipment.

Supporting Information Available: Molecular modeling results for **4a,b**, **5**, **6a,d**, and **7a,b**; ¹H NMR spectra for the compounds **6a,b** and their free amines **7a,b** and free amines **10**, **11**, **12a–d**, **13a,b**, and **14a,b**; ¹H–¹H COSY NMR of free amines of **7a** vs **7b**; elemental analyses for compounds **7a**, **10**, **11**, **12a–d**, **14b**; and X-ray crystallographic data for **12d** are provided. This is available free of charge via the Internet at <http://pubs.acs.org>.

References

- (1) Williams, D. E.; Lassota, P.; Andersen, R. J. Motuporamines A to C, Cytotoxic Alkaloids Isolated from the Marine Sponge *Xestospongia exigua* (Kirkpatrick). *J. Org. Chem.* **1998**, *63*, 4838–4841.
- (2) (a) Williams, D. E.; Craig, K. S.; Patrick, B.; McHardy, L. M.; Soest, R. v.; Roberge, M.; Anderson, R. J. Motuporamines, anti-invasion and anti-angiogenic alkaloids from the marine sponge *Xestospongia exigua* (Kirkpatrick): Isolation, structure elucidation, analogue synthesis, and conformational analysis. *J. Org. Chem.* **2002**, *67*, 245–258. (b) Roskelley, C.; Williams, D. E.; McHardy, L.; Leong, K.; Karsan, A.; Andersen, R. J.; Dedhar, S.; Roberge, M. Inhibition of Tumor Cell Invasion and Angiogenesis by Motuporamines. *Cancer Res.* **2001**, *61*, 6788–6794.
- (3) Kaur, N.; Delcros, J.-G.; Martin, B.; Phanstiel, O., IV. Synthesis and Biological Evaluation of Dihydropotuporamine Derivatives in Cells Containing Active Polyamine Transporters. *J. Med. Chem.* **2005**, *48*, 3832–3839.
- (4) (a) Phanstiel, O., IV; Price, H. L.; Wang, L.; Juusola, J.; Kline, M.; Shah, S. M. The Effect of Polyamine Homologation on the Transport and Cytotoxicity Properties of Polyamine–(DNA-Intercalator) Conjugates. *J. Org. Chem.* **2000**, *65*, 5590–5599. (b) Wang, L.; Price, H. L.; Juusola, J.; Kline, M.; Phanstiel, O., IV. The Influence of Polyamine Architecture on the Transport and Topoisomerase II Inhibitory Properties of Polyamine DNA-Intercalator Conjugates. *J. Med. Chem.* **2001**, *44*, 3682–3691.
- (5) Wang, C.; Delcros, J.-G.; Biggerstaff, J.; Phanstiel, O., IV. Synthesis and Biological Evaluation of N^1 -(anthracen-9-ylmethyl)triamines as Molecular Recognition Elements for the Polyamine Transporter. *J. Med. Chem.* **2003**, *46*, 2663–2671.
- (6) Wang, C.; Delcros, J.-G.; Biggerstaff, J.; Phanstiel, O., IV. Molecular Requirements for Targeting the Polyamine Transport System: Synthesis and Biological Evaluation of Polyamine–Anthracene Conjugates. *J. Med. Chem.* **2003**, *46*, 2672–2682.
- (7) Wang, C.; Delcros, J.-G.; Cannon, L.; Konate, F.; Carias, H.; Biggerstaff, J.; Gardner, R. A.; Phanstiel, O., IV. Defining the Molecular Requirements for the Selective Delivery of Polyamine-Conjugates into Cells Containing Active Polyamine Transporters. *J. Med. Chem.* **2003**, *46*, 5129–5138.
- (8) Gardner, R. A.; Delcros, J.-G.; Konate, F.; Breitbeil, F., III; Martin, B.; Sigman, M.; Phanstiel, O., IV. N^1 -Substituent effects in the selective delivery of polyamine-conjugates into cells containing active polyamine transporters. *J. Med. Chem.* **2004**, *47*, 6055–6069.
- (9) Delcros, J.-G.; Tomasi, S.; Carrington, S.; Martin, B.; Renault, J.; Blagbrough, I. S.; Uriac, P. Effect of spermine conjugation on the cytotoxicity and cellular transport of acridine. *J. Med. Chem.* **2002**, *45*, 5098–5111.
- (10) (a) Bergeron, R. J.; Feng, Y.; Weimar, W. R.; McManis, J. S.; Dimova, H.; Porter, Carl; Raisler, B.; Phanstiel, O. A Comparison of Structure–Activity Relationships between Spermidine and Spermine Analogue Antineoplastics. *J. Med. Chem.* **1997**, *40*, 1475–1494. (b) Kramer, D. L.; Miller, J. T.; Bergeron, R. J.; Khomutov, R.; Khomutov, A.; Porter, C. W. Regulation of polyamine transport by polyamines and polyamine analogues. *J. Cell. Physiol.* **1993**, *155*, 399–407. (c) Bergeron, R. J.; McManis, J. S.; Liu, C. Z.; Feng, Y.; Weimar, W. R.; Luchetta, G. R.; Wu, Q.; Ortiz-Ocasio, J.; Vinson, J. R. T.; Kramer, D.; Porter, C. Antiproliferative Properties of Polyamine Analogues: A Structure–Activity Study. *J. Med. Chem.* **1994**, *37*, 3464–3476. (d) Bergeron, R. J.; Miller, R.; Bussenius, J.; McManis, J. S.; Merriman, R. L.; Smith, R. E.; Yao, H.; Weimar, W. R. Synthesis and Evaluation of Hydroxylated Polyamine Analogues as Antiproliferatives. *J. Med. Chem.* **2000**, *43*, 224–235.
- (11) (a) Cullis, P. M.; Green, R. E.; Merson-Davies, L.; Travis, N. Probing the mechanism of transport and compartmentalisation of polyamines in mammalian cells. *Chem. Biol.* **1999**, *6*, 717–729 and refs therein. (b) Seiler, N.; Dezeure F. Polyamine transport in mammalian cells. *Int. J. Biochem.* **1990**, *22*, 211–218. (c) Seiler, N.; Delcros, J.-G.; Moulinoux, J. P. Polyamine Transport in Mammalian Cells. An Update. *Int. J. Biochem. Cell. Biol.* **1996**, *28*, 843–861.
- (12) Covassin, L.; Desjardins, M.; Charest-Gaudreault, R.; Audette, M.; Bonneau, M. J.; Poulin, R. Synthesis of spermidine and norspermidine dimers as high affinity polyamine transport inhibitors. *Bioorg. Med. Chem. Lett.* **1999**, *9*, 1709–1714.
- (13) Wang, C.; Abboud, K. A.; Phanstiel, O., IV. Synthesis and Characterization of N^1 -(4-toluenesulfonyl)- N^1 -(9-anthracenemethyl)-triamines. *J. Org. Chem.* **2002**, *67*, 7865–7868.
- (14) (a) Gardner, R. A.; Kinkade, R.⁺; Wang, C.; Phanstiel, O., IV. Total Synthesis of Petrobactin and Its Homologues as Potential Growth Stimuli for *Marinobacter hydrocarbonoclasticus*, an oil-degrading bacteria. *J. Org. Chem.* **2004**, *69*, 3530–3537. (b) Kuksa, V.; Buchan, R.; Lin, P. K. T. Synthesis of Polyamines, Their Derivatives, Analogues and Conjugates. *Synthesis* **2000**, 1189–1207. (c) Bergeron, R. J.; Bharti, N.; Wiegand, J.; McManis, J. S.; Yao, H.; Prokai, L. Polyamine-Vectored Iron Chelators: The Role of Charge. *J. Med. Chem.* **2005**, *48*, 4120–4137.
- (15) (a) Aikens, D.; Bunce, S.; Onasch, F.; Parker, R.; Hurwitz, C.; Clemans, S. The Interactions between Nucleic Acids and Polyamines II. Protonation Constants and ¹³C NMR Chemical Shift Assignments of Spermidine, Spermine and Homologs. *Biophys. Chem.* **1983**, *17*, 67–74. (b) Onasch, F.; Aikens, D.; Bunce, S.; Schwartz, H.; Nairn, D.; Hurwitz, C. The Interactions between Nucleic Acids and Polyamines III. Microscopic Protonation Constants of Spermidine. *Biophys. Chem.* **1984**, *19*, 245–253.
- (16) Data from http://www.aist.go.jp/RIODB/SDBS/cgi-bin/cre_index.cgi. This is a free site organized by National Institute of Advanced Industrial Science and Technology (AIST), Japan, for spectra of known compounds.
- (17) (a) Burley S. K.; Petsko G. A. Amino-aromatic interactions in proteins. *FEBS Lett.* **1986**, *203*, 139–143. (b) Perutz, M. F. The role of aromatic rings as hydrogen-bond acceptors in molecular recognition. *Philos. Trans. R. Soc. Ser. A* **1993**, *345*, 105–112. (c) Gallivan, J. P.; Dougherty, D. A. Cation- π interactions in structural biology. *Proc. Natl. Acad. Sci. U.S.A.* **1999**, *96*, 9459–9464.

JM050814W